Macromolecules

pubs.acs.org/Macromolecules Article

Surface Segregation in Athermal Polymer Blends Due to Conformational Asymmetry

Russell K. W. Spencer* and Mark W. Matsen*

Cite This: *Macromolecules* 2021, 54, 10100−10109 Read Online

ACCESS | Metrics & More | Article Recommendations

ABSTRACT: Monte Carlo simulations are used to investigate the surfaces of athermal blends of stiff and flexible polymers as the bending modulus of the stiff polymers, κ, is increased from zero to the point where the bulk undergoes an isotropic−nematic transition. For hard walls characteristic of polymer/solid surfaces, the flexible polymers generally segregate to the surface. However, just prior to the bulk transition, a surface transition occurs where a thin nematic layer rich in stiff polymers forms next to the wall. This appears to be followed by a second surface transition where the degree of order abruptly increases, which, in turn, causes a rapid thickening of the nematic layer that nucleates the bulk nematic phase. For soft boundaries representative of polymer/air surfaces, a thin layer rich in stiff polymers but without nematic order forms on the outer edge of the surface with a more significant layer rich in flexible polymers beneath. In this case, the surface transitions are lost and the qualitative behavior remains unchanged as κ increases.

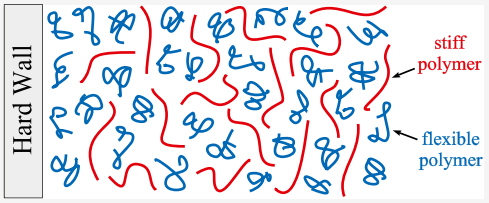

INTRODUCTION

The blending of polymers provides a simple means of tailoring material properties. However, it can also complicate surface properties, which are important for many technological applications such as adhesion, lubrication, wetting, colloidal stabilization, catalysis, material processing, and protein adsorption.[1] Naturally, surface behavior will generally depend on both enthalpic and entropic effects, but it is usually the enthalpy that dominates. As a result, the role of entropy is not particularly well understood.

One exception is the entropic tendency for smaller molecules to segregate to a surface, which becomes relevant when blending two different molecular weights of the same polymeric species. The effect originates from an entropic preference for chain ends at the surface, which, in turn, favors small molecules on account of the fact that they have more ends per unit volume of material. This has been well confirmed by simulations,[2−7] theory,[8−13] and experiments.[14,15] Nevertheless, the underlying reason for ends to favor the surface is not intuitive. Silberberg[16] showed that for an incompressible melt of flexible polymers, a hard wall acts like a reflecting boundary, which implies that the distribution of chain ends should not be affected by the surface. It is, in fact, deviations from the assumptions of the Silberberg argument, such as a finite width of the surface or a limited flexibility of the polymers, that cause the segregation.[11,13]

Another entropic effect is that of conformational asymmetry. It was first noticed by Sikka et al.[17,18] in experiments on a series of polyolefin diblock copolymers, where the two components were chemically similar but with considerably different statistical segment lengths. Note that the comparison is for segments of equal molecular volume. The experiments observed that the diblock copolymers always ordered with the shorter segment length component at the polymer/air and polymer/solid surfaces. Subsequent experiments by Scheffold et al.[19] on binary polyolefin blends also found that the shorter segment length component segregated to polymer/air surfaces, although they were unable to detect any preference at polymer/solid surfaces. Similar experiments by Tretinnikov and Ohta[20,21] examined blends of isotactic and syndiotactic PMMA, where the polymers are chemically identical but linked together differently resulting in a shorter statistical segment length for the syndiotactic version. Again, it was the shorter segment length component that segregated to the polymer/air and polymer/solid surfaces. Despite the chemical similarity of the components, there still remains a question of whether the experiments are free of significant enthalpic effects.[19−22]

Theory and simulations have the distinct advantage that they can ensure there is no enthalpic bias. That does not, however, mean that their behavior will be strictly entropic. Models will still generally include monomer−monomer interactions, monomer−surface interactions, and/or molecular bending energies. What the models are able to ensure is that the blends are athermal in that the surface has no energetic preference for either component and the nonbonded interactions between all

Received: August 26, 2021
Revised: October 8, 2021
Published: October 19, 2021

https://doi.org/10.1021/acs.macromol.1c01805
Macromolecules 2021, 54, 10100−10109

monomers are identical. Despite this advantage, theory and simulations have actually confused the issue.

Density functional theories (DFTs) by Fredrickson and Donley[23] and by Tripathi and Chapman,[24] as well as self-consistent field theory (SCFT) by Donley and Fredrickson[25] and by Wu et al.,[26] predict that the more compact component with the shorter statistical segment length segregates to the surface. However, Monte Carlo (MC) simulations by Kumar, Yethiraj, and co-workers[22,27] of binary blends of flexible and stiff polymers next to hard walls observed a general preference for the stiff polymers, which is the less compact component. They speculated that the preference for stiff chains was due to packing effects, which are not accounted for by calculations that employ the mean-field approximation or that model polymers as flexible Gaussian chains. However, mean-field-type calculations on semiflexible polymers by Carignano and Szleifer[28] found examples where the stiff chains are preferred at surfaces, while Stepanow and Fedorentko[29] found that fluctuation corrections to the SCFT of Gaussian chains lead to a preference for the component with the longer segment length. To complicate the issue even further, Yethiraj[30] showed that simply modifying athermal interactions with the wall or between monomers can reverse the surface segregation. There are also more recent molecular dynamics (MD) simulations on diblock copolymer melts by Nikoubashman et al.,[32] which reported a preference for the component with the shorter statistical segment length, even in the athermal limit (i.e., $\chi = 0$) where the structureless disordered melt resembles a binary blend.

The aim of this study is to better understand the role of packing effects, which tend to align polymer chains, and to determine the extent to which they may invalidate calculations based on Gaussian chains and/or the mean-field approximation. To do so, we perform MC simulations on blends of freely jointed polymers and semiflexible polymers with an adjustable bending modulus, κ. Our simulations are analogous to those of Kumar et al.,[22,27] except that we restrict the polymers to a lattice to increase the computational efficiency. The blends are completely athermal to ensure that there is no enthalpic bias, and the molecular volumes of the flexible and stiff polymers are identical to exclude size-related segregation. We expect that packing effects will be reduced for polymer/air surfaces, and so we examine segregation next to soft surfaces as well as hard walls.

MONTE CARLO SIMULATION

The blends in our study contain n polymers of which n_s are stiff and $n_f = n - n_s$ are flexible. To avoid entropic segregation due to size disparity, both polymers have an equal number of monomers labeled by $i = 1, 2, 3, ..., N$. The stiff polymers are labeled by $j = 1, 2, ..., n_s$, and the flexible polymers are labeled by $j = n_s + 1, n_s + 2, ..., n$. The position of monomer i of polymer j is denoted by the vector $\mathbf{r}_i^{(j)}$, as depicted in Figure 1. For computational efficiency, the monomers are restricted to the sites of a lattice with a maximum of one monomer per site and bonded monomers occupying nearest-neighbor sites. To allow room for the polymers to move, we generally leave 20% of the sites vacant, and to minimize lattice effects, we choose an fcc lattice with a large coordination number of 12. It is constructed by taking a simple cubic $L_x \times L_y \times L_z$ lattice with a lattice spacing of d and deleting every second site leaving $M = L_xL_yL_z/2$ sites with a nearest-neighbor spacing (and thus polymer bond length) of $b = \sqrt{2}\,d$. The conformational asymmetry is introduced by applying a bending energy of

$$E_{\text{bend}} = -\kappa \sum_{j=1}^{n_s} \sum_{i=1}^{N-1} \mathbf{u}_i^{(j)} \cdot \mathbf{u}_{i+1}^{(j)} \tag{1}$$

to the stiff chains, where κ is the bending modulus and $\mathbf{u}_i^{(j)} \equiv [\mathbf{r}_{i+1}^{(j)} - \mathbf{r}_i^{(j)}]/b$ are unit vectors denoting the bond orientations, as illustrated in Figure 1.

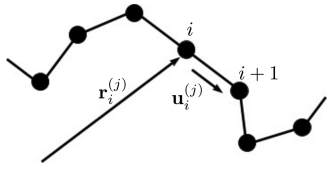

Figure 1. Illustration showing a portion of the jth polymer. The position of the ith monomer is denoted by the vector $\mathbf{r}_i^{(j)}$, and the orientation of its bond with the $(i + 1)$th monomer is denoted by the unit vector $\mathbf{u}_i^{(j)}$.

Our MC simulations of the model attempt, with equal probability, reptation and crank-shaft trial moves, analogous to those used by Kumar et al.[22,27] As detailed in ref 33, the reptation trial randomly selects one of the $2n$ end monomers and one of its 12 nearest-neighbor sites to move to, while the crank-shaft trial randomly selects one of the $(N-2)n$ middle monomers and one of the potential sites that can be reached without moving its two bonded neighbors. Each move is immediately rejected if it results in the double occupancy of a site. Otherwise, the move is accepted or rejected based on the standard Metropolis criterion. We do not include the swap move between flexible and stiff chains used by Kumar et al. Although this trial move would be effective when κ and N are small, the acceptance rate would inevitably vanish for large κ and N, where nonequilibrium effects are most serious. In our simulations, nonequilibrium issues are considerably reduced using a lattice model with a modest polymerization of $N = 40$. Nevertheless, we still apply a generous number of MC steps to equilibrate our blends (typically 10^5–10^6 per monomer) and likewise a large number of MC steps to evaluate ensemble averages (typically 10^5–10^7 per monomer).

BULK BEHAVIOR

For simplicity, we limit our study to the surfaces of isotropic blends of 50–50 composition, and so we need to ensure κ is small enough that the bulk region does not develop nematic order. We also need to know how κ affects the conformational asymmetry between the stiff and flexible polymers. Therefore, we begin by examining the effect of κ on bulk behavior. This is done by simulating equal numbers of stiff and flexible polymers (i.e., $n_s = n_f$) of equal polymerization $N = 40$ in a cubic simulation box of size $L_\alpha = 60$ ($\alpha = x$, y, and z) with periodic boundary conditions and an average monomer density of $\phi_{\text{bulk}} = nN/M = 0.8$.

To detect the bulk isotropic–nematic transition, we sample the distribution of bond orientations among the stiff chains

$$\hat{p}(\mathbf{u}) = \frac{1}{n_s(N-1)} \sum_{j=1}^{n_s} \sum_{i=1}^{N-1} \delta(\mathbf{u} - \mathbf{u}_i^{(j)}) \tag{2}$$

From its ensemble average, $p(\mathbf{u}) \equiv \langle \hat{p}(\mathbf{u}) \rangle$, we obtain the Q-tensor

$$Q_{\alpha\beta} = \frac{3}{2} \sum_{\mathbf{u}} p(\mathbf{u}) \left[u_\alpha u_\beta - \frac{1}{3}\delta_{\alpha\beta} \right] \tag{3}$$

https://doi.org/10.1021/acs.macromol.1c01805
Macromolecules 2021, 54, 10100–10109

where u_α is the α-component of the bond orientation, **u**. The tensor is symmetric and traceless, and as such, it reduces to the diagonal form

$$Q_{\alpha\beta} = \frac{3}{2}S\left(n_\alpha n_\beta - \frac{1}{3}\delta_{\alpha\beta}\right) + \frac{1}{2}P(m_\alpha m_\beta - l_\alpha l_\beta) \quad (4)$$

where **l**, **m**, and **n** are orthonormal eigenvectors. The largest eigenvalue defines the uniaxial order parameter, S, which varies from 0 to 1. A value of $S \neq 0$ signifies orientational order. The preferred orientation of the bonds is then given by the corresponding eigenvector, **n**, which is referred to as the nematic director. The difference between the two smallest eigenvalues defines the biaxial order parameter, P, which varies from 0 to $3S$. At the upper limit of $S = P/3$, the two largest eigenvalues become degenerate and thus there is no longer a single preferred orientation of the bonds.

Figure 2 plots the order parameter, S, of the stiff polymers as a function of their bending modulus, κ, from two different sets of

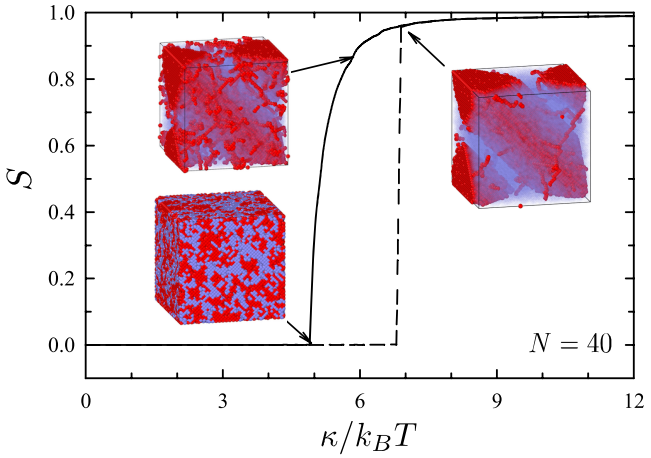

Figure 2. Nematic order parameter, S, of the stiff polymers plotted as a function of their bending modulus, κ. The dashed and solid curves are for simulations initialized with equilibrated configurations from κ/k_BT = 0 and 12, respectively. The insets show configurations of the stiff (red) and flexible (blue) polymers in a homogeneous isotropic state and two demixed isotropic−nematic states with weak and strong order.

simulations. The first set is initialized with an isotropic configuration corresponding to κ = 0. In this case, the blend remains isotropic up until $\kappa \approx 6.8k_BT$, beyond which S jumps to a value close to one. Visual inspection of the configurations (see the inset on the right) reveals that the blend macrophase separates, forming a cylindrical nematic domain consisting of mostly stiff polymers in fully extended conformations coexisting with an isotropic phase rich in flexible polymers. The second set of simulations is initialized with a macrophase-separated configuration from the first set of simulations at $\kappa = 12k_BT$. In this case, the nematic order decreases continuously to the fully isotropic state at $\kappa \approx 4.9k_BT$ (see the insets on the left). Hence, we expect the true bulk transition to be somewhere in the interval from 4.9 to $6.8k_BT$. Subsequent results, to be discussed shortly, find that the transition is close to the lower bound, implying that it is weakly first-order as is usually the case for isotropic−nematic transitions.[31]

To assess the degree of conformational asymmetry, Figure 3 compares the average end-to-end lengths, R_0, of the stiff and flexible polymers. More specifically, it plots the ratio $R_0/N^{1/2}$, which converges to the statistical segment length, a, in the limit

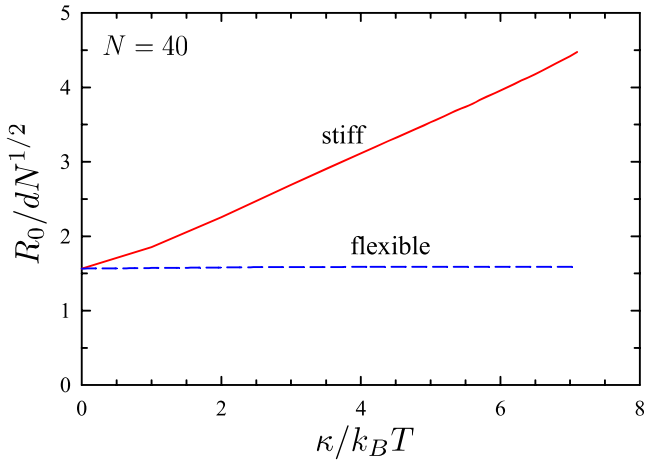

Figure 3. Average end-to-end lengths, R_0, of the stiff (solid curve) and flexible (dashed curve) polymers in the bulk isotropic phase plotted as a function of the bending modulus, κ, of the stiff polymers.

of $N \to \infty$. Although our polymers are finite (i.e., N = 40), the ratio should still provide a reasonable estimate of a. Indeed, our value of $R_0/N^{1/2} = 1.57d$ for neat melts of flexible chains (i.e., κ = 0) is comparable to the accurate value of $a = 1.74d$ obtained from an extrapolation to infinite N.[34] Thus, based on R_0, the statistical segment length of the stiff polymers increases almost linearly with κ, while that of the flexible polymers remains virtually constant despite the changing environment.

The statistical segment lengths can potentially be affected by the composition of the blend. To test this possibility, we ran simulations with compositions ranging from that of a single stiff chain in a sea of flexible chains (i.e., n_s = 1) to that of a single flexible chain in a sea of stiff chains (i.e., $n_s = n - 1$). We found no significant effect on the R_0 of the stiff chains provided they remain in the isotropic phase. The most significant effect was on the R_0 of the flexible chains, which increased up to 10% when immersed in a sea of stiff chains just prior to the onset of nematic order. Even still, this change is negligible compared to the threefold difference between the segment lengths of the stiff and flexible chains.

HARD WALL

Having examined the bulk behavior, we now turn our attention to the surface segregation of an isotropic blend (i.e., $\kappa \lesssim 5k_BT$) next to a hard wall. The wall is created by prohibiting the occupation of sites in a particular z layer of the lattice, which reduces the available number of sites to $M = L_xL_y(L_z - 1)/2$. Naturally, the wall will perturb the total polymer concentration but more so than in real systems because our model lacks the attractive interactions that tend to maintain a uniform bulk concentration. To compensate for this, we follow the strategy in ref 7 where a surface field, $w(z)$, is introduced to create a step profile. The energy of the field is given by

$$E_w = \frac{L_xL_y}{2}\sum_z w(z)[\hat{\phi}_s(z) + \hat{\phi}_f(z)] \quad (5)$$

where

$$\hat{\phi}_s(z) = \frac{2}{L_xL_y}\sum_{j=1}^{n_s}\sum_{i=1}^{N}\delta(z - z_i^{(j)}) \quad (6)$$

https://doi.org/10.1021/acs.macromol.1c01805
Macromolecules 2021, 54, 10100−10109

$$\hat{\phi}_f(z) = \frac{2}{L_x L_y} \sum_{j=n_s+1}^{n} \sum_{i=1}^{N} \delta(z - z_i^{(j)}) \quad (7)$$

are the instantaneous concentration profiles of the stiff and flexible polymers, respectively. Here, $z_i^{(j)}$ is the z component of the position vector $\mathbf{r}_i^{(j)}$. The field, $w(z)$, is adjusted during the equilibration period, as described in ref 7, until the total ensemble-average concentration is uniform (i.e., $\phi_s(z) + \phi_f(z) = \phi_{bulk} = 0.8$).

Figure 4 displays a sample configuration for $\kappa = 4.6k_BT$, where the stiff and flexible polymers are shown in red and blue,

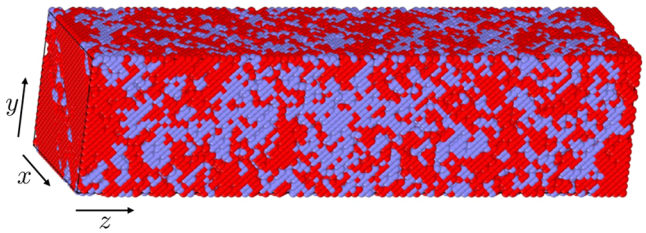

Figure 4. Equilibrated configuration of flexible polymers (blue) and stiff polymers of $\kappa = 4.6k_BT$ (red) in a simulation box with periodic boundaries in the x and y directions and hard walls at the two ends in the z direction.

respectively. To alleviate confinement effects due to the wall, the simulation box was given a large z dimension ($L_z = 160$) relative to its cross-sectional size ($L_x = L_y = 40$). The image reveals visible segregation of stiff polymers to the two ends of the simulation box next to the hard walls, which causes a slight depletion in the bulk region on account of the finite size of our simulation box. To compensate for this finite-size effect, the number of stiff polymers ($n_s = 1333$) was increased relative to the number of flexible polymers ($n_f = 1211$) so as to restore the 50−50 composition in the bulk.

The surface segregation progresses through three distinct stages as the bending modulus, κ, of the stiff polymers is increased. Examples of the concentration profiles, $\phi_s(z)$ and $\phi_f(z)$, are plotted in Figure 5 for $\kappa/k_BT = 2.0$, 4.0, and 4.6. To assess the degree of chain packing, Figure 6 plots the order parameters, $S(z)$ and $P(z)$, of the stiff chains as a function of distance from the wall. The z-dependent order parameters are calculated using the same expression as for the bulk (eq 3) except that the distribution of bond orientations, $p(\mathbf{u}, z)$, is evaluated separately for each lattice layer, z. In particular, the bonds are weighted according to how many ends they have in layer z, and the distribution is normalized such that $\sum_{\mathbf{u}} p(\mathbf{u}, z) = 1$ for each value of z.

At the lower value of $\kappa = 2k_BT$, the average end-to-end lengths of the flexible and stiff polymers from Figure 3 are $R_0 = 10.0d$ and $14.3d$, respectively. This conformational asymmetry is almost identical to that of the MD simulations by Nikoubashman et al.[32] and comparable to the asymmetries investigated in the experiments of Sikka et al.[17,18] Consistent with both, we observe a surface preference for the more compact (i.e., more flexible) polymers. Furthermore, our results are in good agreement with the SCFT calculation of Wu et al.[26] which predicts the excess to decay proportional to

$$F_\rho(Z) = \frac{(1 + Z^2)}{\sqrt{\pi}} \exp(-Z^2) - \left(\frac{3Z}{2} + Z^3\right) \mathrm{erfc}(Z) \quad (8)$$

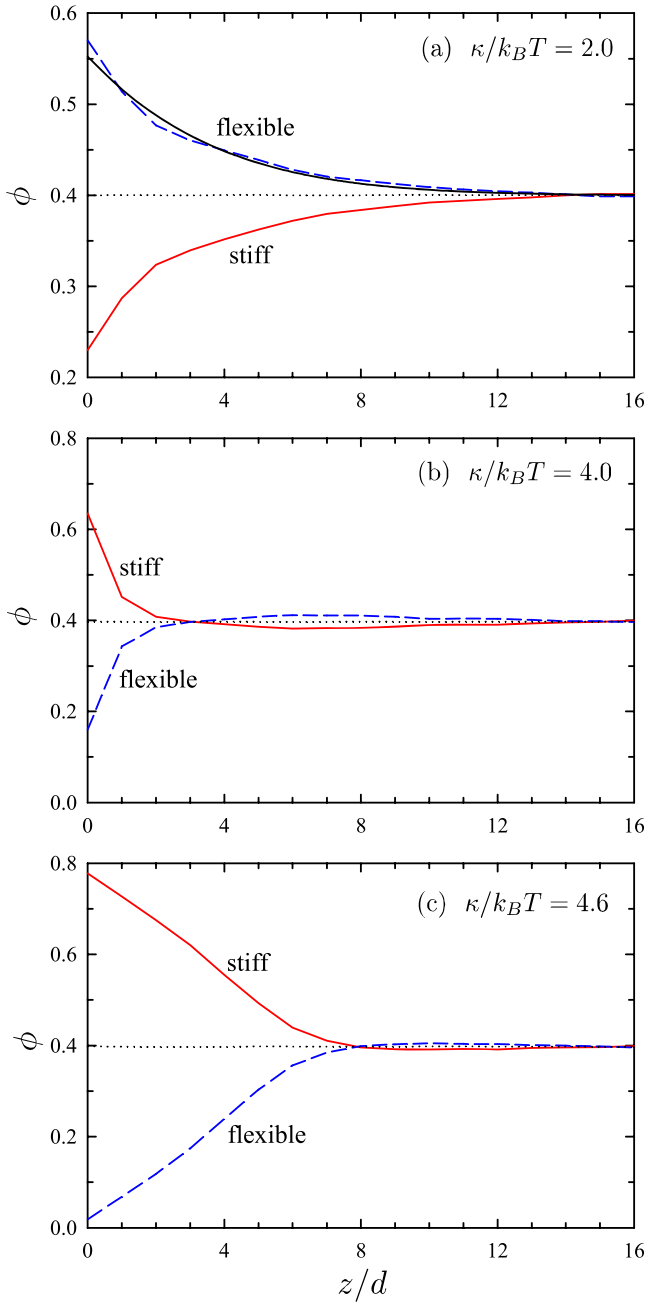

Figure 5. Ensemble-average concentrations of stiff polymers, $\phi_s(z)$ (solid curve), and flexible polymers, $\phi_f(z)$ (dashed curve), next to a hard wall at $z = 0$ evaluated for (a) $\kappa = 2k_BT$, (b) $\kappa = 4k_BT$, and (c) $\kappa = 4.6k_BT$. The dotted lines denote the average concentration, $[\phi_s(z) + \phi_f(z)]/2$, corresponding to no segregation, and the black curve in panel (a) plots the fit $\phi_f(z) = 0.27F_\rho(Z) + 0.4$.

where $Z = \sqrt{3/2}\, z/\bar{R}_0$ and $\bar{R}_0^2$ is the average of the squared end-to-end lengths of the flexible and stiff polymers. Indeed, the fit $\phi_f(z) = 0.27F_\rho(Z) + 0.4$, shown by the black curve in Figure 5a, agrees well with our simulation results. Note that the predicted profile assumes small conformational asymmetry and consequently it becomes inaccurate if $\kappa \gtrsim 3k_BT$. Figure 6a reveals a small degree of orientational order among the stiff chains at the surface ($z = 0$), which incidentally is also present for the flexible chains. This is because the wall precludes 4 of the nonparallel bond orientations out of the 12 possible orientations. Nevertheless, the fact that $S(0) = P(0)/3$ implies that there is no

https://doi.org/10.1021/acs.macromol.1c01805
Macromolecules 2021, 54, 10100−10109

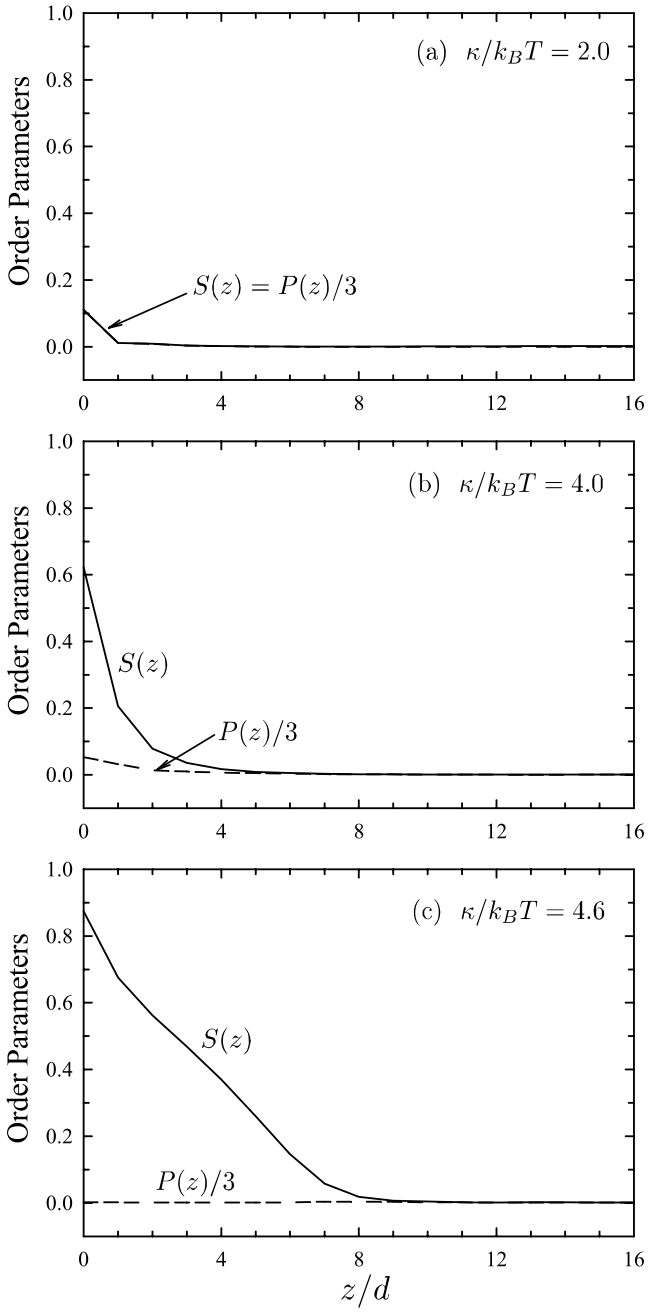

Figure 6. Nematic order parameter, $S(z)$ (solid curves), and biaxial order parameter, $P(z)$ (dashed curves), of the stiff polymers evaluated for (a) $\kappa = 2k_BT$, (b) $\kappa = 4k_BT$, and (c) $\kappa = 4.6k_BT$. In all cases, the nematic director, **n**, is parallel to the wall.

preferred bond orientation within the $x-y$ plane and thus no nematic order. Furthermore, the orientational order virtually vanishes in the neighboring lattice layer ($z = d$), implying that there are no significant packing effects between the polymers.

At the intermediate value of $\kappa = 4k_BT$ in Figure 5b, we obtain results similar to those of Kumar et al.[22,27] Here, a thin wetting layer rich in stiff polymers forms next to the wall, beyond which there remains a slight preference for the flexible polymers that decays to zero on a length scale of $\bar{R}_0$. Figure 6b also reveals significant packing effects in the wetting layer, sufficient to induce nematic order (i.e., $S(z) > P(z)/3$). However, at this value of κ, the average end-to-end lengths of the flexible and stiff polymers are $R_0 = 10.5d$ and $19.7d$, respectively, which corresponds to a conformational asymmetry well beyond that of the simulations by Kumar et al.[22]

The segregation of stiff chains becomes considerably more pronounced at $\kappa = 4.6k_BT$. In Figure 5c, the surface is nearly pure in stiff chains and the preference extends much further into the melt. Likewise, Figure 6c reveals that the nematic order parameter at the surface is nearly one (i.e., $S(0) \approx 1$) with a decay that closely tracks the excess concentration (i.e., $S(z) \propto \phi_s(z) - 0.4$). Even still, though, there remains a region deeper inside the melt ($8d \lesssim z \lesssim 14d$) where the flexible chains are slightly preferred.

To follow the evolution of the entropic segregation as a function of κ, we examine several different surface properties in Figure 7. The upper plot shows the excess of stiff chains

$$\phi_{ex}(z) = \frac{1}{2}[\phi_s(z) - \phi_f(z)] \tag{9}$$

at $z = 0$, and the middle plot shows the integrated excess

$$\Gamma_{ex} = \frac{1}{2}\sum_z \phi_{ex}(z) \tag{10}$$

The factor of half in eq 10 accounts for the fact that there are two surfaces, one at each end of the simulation box. Finally, the lower plot shows the orientational order parameters of the stiff chains adjacent to the wall, $S(0)$ and $P(0)$. These results reveal clear evidence for a surface transition at $\kappa \approx 3.9k_BT$ and compelling evidence for a second surface transition at $\kappa \approx 4.5k_BT$.

The first surface transition results in the formation of a thin nematic layer at the wall, breaking the rotational symmetry in the $x-y$ plane as signified by the fact that $S(0) > P(0)/3$. This is analogous to the surface transition studied by Ivanov et al.[35] in semidilute solutions of semiflexible polymers using MC simulations of the bond-fluctuation model. They likewise observed a sharp increase in the nematic order parameter similar to that at $\kappa \approx 3.9k_BT$ in Figure 7c. Although the sharp increase seemed to suggest a first-order transition, their careful analysis concluded that the transition was actually second-order. The same is presumably true here. Note that the slight degree of broken symmetry that occurs just prior to the transition at $\kappa \approx 3.8k_BT$ can be attributed to the bond correlation length in the $x-y$ plane exceeding the dimensions of the simulation box (i.e., L_x and L_y). In the absence of finite-size effects, the symmetry breaking would coincide precisely with the critical surface transition.

The second surface transition resembles a classical prewetting transition,[36] where the degree of order and thickness of the wetting layer increase discontinuously. Indeed, Figure 7a shows that the relative concentration of stiff chains at the surface, $2\phi_{ex}(0)/\phi_{bulk}$, jumps from about 77 to 95%, which is accompanied in Figure 7c by a noticeable jump in the nematic order parameter, $S(0)$. The more striking effect, however, involves the integrated excess of stiff chains, Γ_{ex}, plotted in Figure 7b. In particular, Γ_{ex} switches from a relatively weak dependence on κ prior to the transition to a far stronger dependence after the transition. This is caused by a rapid divergence in the thickness of the nematic layer, which then nucleates nematic order in the bulk region. It is this nucleation that provides the more accurate estimate of $\kappa \approx 5k_BT$ for the bulk isotropic–nematic transition mentioned in the preceding section.

https://doi.org/10.1021/acs.macromol.1c01805
Macromolecules 2021, 54, 10100−10109

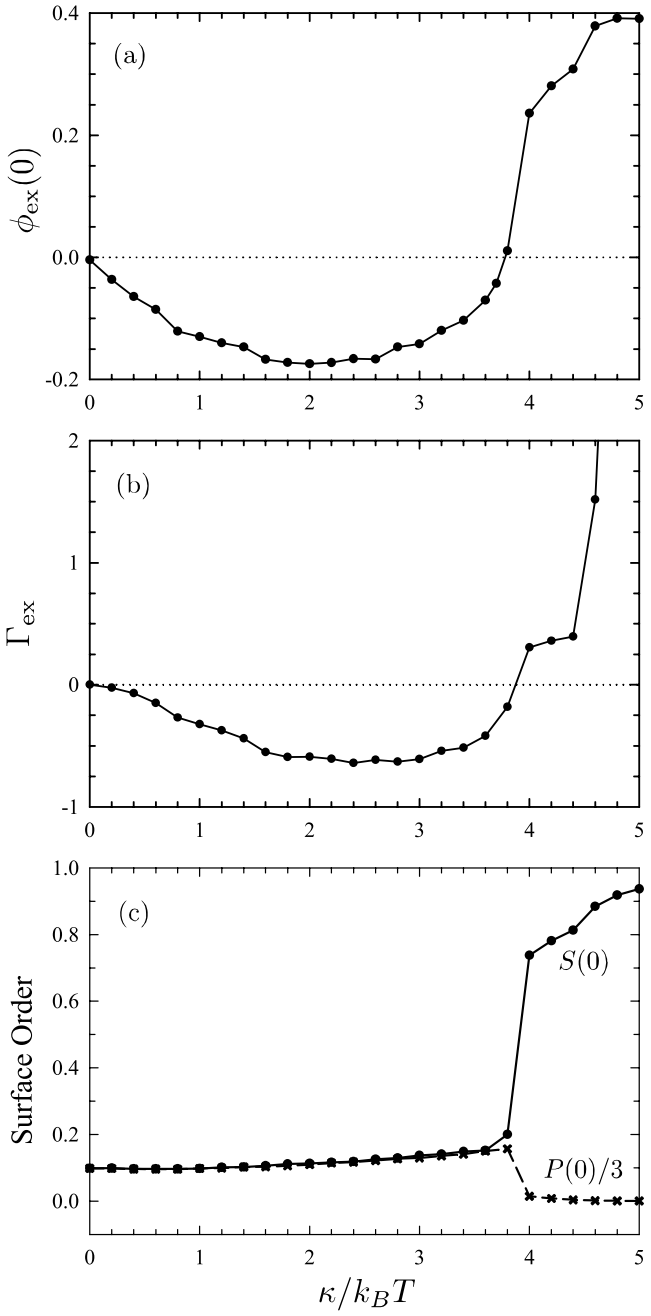

Figure 7. (a) Excess concentration of stiff polymers adjacent to the surface, $\phi_{ex}(0)$, (b) integrated excess of stiff chains, Γ_{ex}, and (c) orientational order parameters adjacent to the surface, $S(0)$ and $P(0)$, plotted as functions of the bending modulus of the stiff chains, κ.

SOFT SURFACE

Here, we switch to a soft surface that mimics the behavior of a polymer blend in contact with air. This is done by adjusting $w(z)$ so that the total polymer concentration, $\phi_s(z) + \phi_f(z)$, adopts the gradual profile

$$\phi_t(z) = \frac{\phi_{bulk}}{2}\left[\tanh\left(\frac{2z}{w_s}\right) - \tanh\left(\frac{2(z-L_0)}{w_s}\right)\right] \quad (11)$$

corresponding to two surfaces of width w_s located at $z = 0$ and $z = L_0$. Here, we assume a sigmoidal shape for the surface profiles as obtained from detailed simulations that include the necessary cohesive attraction among the polymers required to produce a polymer/air surface.[37,38] One can regard the $w(\mathbf{r})$ in the present simulations as a mean-field approximation for the cohesive forces missing from our model.[13] The following simulations are all performed with $\phi_{bulk} = 0.8$, $w_s = 4d$, and $L_0 = 86d$.

Figure 8 displays a sample configuration for $\kappa = 4k_BT$, with the stiff and flexible polymers shown in red and blue, respectively.

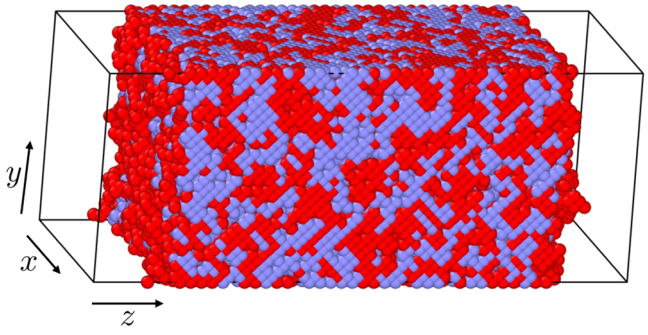

Figure 8. Sample configuration of flexible polymers (blue) and stiff polymers of $\kappa = 4k_BT$ (red) from a simulation box with periodic boundaries in the x and y directions and soft surfaces at the two ends in the z direction.

The average concentrations of the two components, $\phi_s(z)$ and $\phi_f(z)$, are plotted in Figure 9. Unlike before, the qualitative

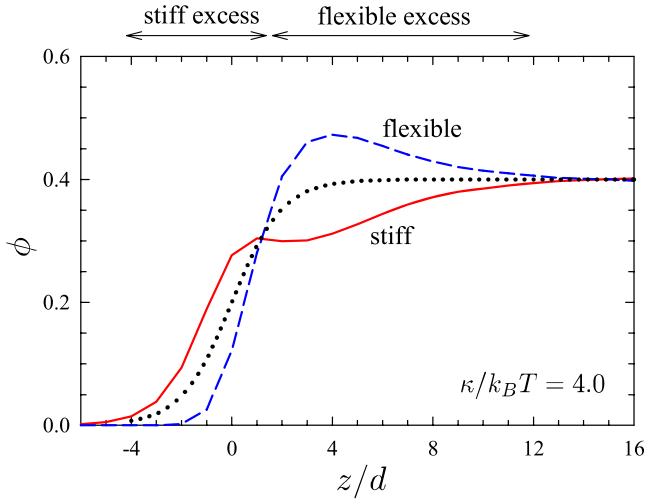

Figure 9. Analogous plot to Figure 6b but for a gradual surface profile as indicated by the dotted curve. The intervals at the top denote an outer region rich in stiff polymers (i.e., $\phi_{ex}(z) > 0$) and an inner region rich in flexible polymers (i.e., $\phi_{ex}(z) < 0$).

behavior remains the same over the entire range of κ. In all cases, there is an excess of stiff polymers in the outer region of the surface ($z \lesssim 0$) that switches to an excess of flexible polymers as the total concentration approaches the bulk value ($z \gtrsim 0$). The excess of flexible polymers again decays with a profile proportional to eq 8, provided $\kappa \lesssim 3k_BT$.

Figure 10 plots the order parameters of the stiff chains, $S(z)$ and $P(z)$. Although their values are exceptionally small, they do nevertheless reveal important clues to the behavior. The region rich in stiff chains has an outer part ($z \ll 0$), where $S(z) > 0$ and $P(z) = 0$ with the nematic director, $\mathbf{n}$, oriented normal to the surface, and an inner part ($z \lesssim 0$), where $S(z) = P(z)/3$ with $\mathbf{n}$ parallel to the surface. In the region rich in flexible chains ($z \gtrsim$

https://doi.org/10.1021/acs.macromol.1c01805
Macromolecules 2021, 54, 10100−10109

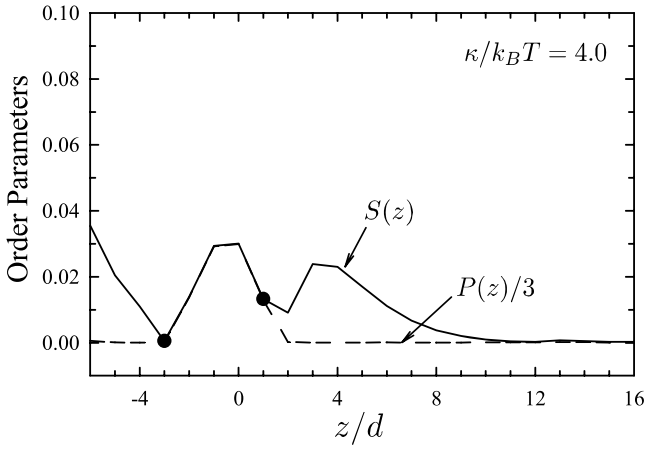

Figure 10. Analogous plot to Figure 7b but for a gradual surface profile. The nematic director, **n**, is parallel to the surface in the interval between the dots and perpendicular to the surface outside the interval.

0), the order parameters switch back to $S(z) > 0$ and $P(z) = 0$ with **n** again perpendicular to the surface.

These observations suggest that as stiff polymers encounter the surface they generally bend parallel to it, which accounts for the interval near the surface ($z \approx 0$) where **n** is parallel. Despite this tendency to orient parallel, the concentration of stiff polymers is too low to develop sufficient orientational order to break the rotational symmetry in the $x-y$ plane, as confirmed by the fact that $S(0) = P(0)/3$. In cases where the length of stiff chain near the surface is relatively short, the end of the polymer will simply stick out of the surface rather than incur a bending penalty, which explains the extreme outer region ($z \ll 0$) where **n** is normal to the surface. This latter assertion is supported by the existence of a relatively large population of chain ends from the stiff polymers (not shown).

The integrated excess of stiff polymers defined in eqs 9 and 10 is plotted in Figure 11. The inset confirms that the excess vanishes in the limit of $\kappa \to 0$, as it must when both polymers become equivalent. To help clarify the behavior, Figure 11 separates the total excess, $\Gamma_{ex} = \Gamma_+ + \Gamma_-$, into the contributions,

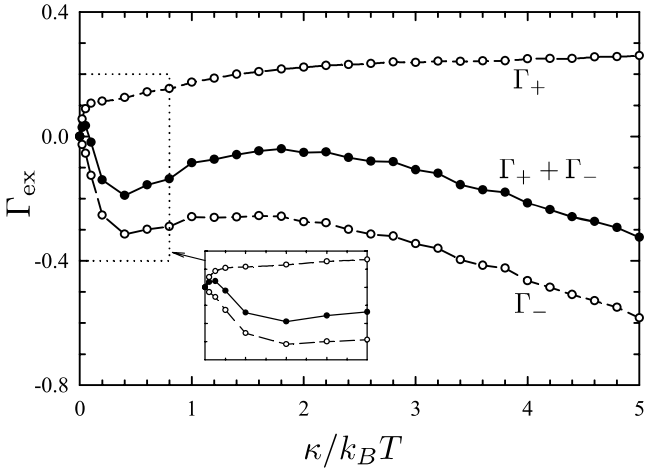

Figure 11. Integrated excess of stiff polymers as a function of their bending modulus, κ (solid curve). The dashed curves show the contributions, Γ_+ and Γ_-, from the outer and inner regions denoted in Figure 9, where $\phi_{ex}(z)$ is positive and negative, respectively. The inset shows an expanded view of the boxed region near $\kappa = 0$.

Γ_+ and Γ_-, from the outer region where $\phi_{ex}(z) > 0$ and the inner region where $\phi_{ex}(z) < 0$, respectively. As κ increases, Γ_+ saturates while the magnitude of Γ_- increases monotonically. With the exception of very small κ, the segregation of flexible polymers in the inner region dominates the segregation of stiff polymers in the outer region. Unlike the hard wall, the curves show no evidence of any surface transitions. Furthermore, we are able to push κ to values beyond the bulk isotropic–nematic transition because the surface no longer nucleates the nematic phase.

DISCUSSION

Our lattice MC simulations find, even for a hard wall, that packing effects are not critically important for typical degrees of conformational asymmetry (i.e., $\kappa \lesssim 2k_BT$). As we have already pointed out, this is supported by the fact that the bond alignment induced by the wall at $z = 0$ essentially vanishes for $z > 0$ (see Figure 6a). Thus, DFT and SCFT should be able to provide reliable predictions for the entropic surface segregation of conformationally compact polymers observed in experiments.[17−21] This is supported by the fact that the segregation of flexible polymers in our simulations (see Figures 5a and 12a) conforms to the SCFT prediction in eq 8.[26]

Packing effects do, however, become important as the first surface transition at $\kappa \approx 3.9k_BT$ is approached. This is reflected by the fact that $S(z)$ and $P(z)$ acquire appreciable values beyond $z = 0$. There is also the slight breaking of rotational symmetry about the z axis (i.e., $S(0) \gtrsim P(0)/3$) at $\kappa = 3.8k_BT$ in Figure 7c, which we attributed to the finite correlation length of the bond

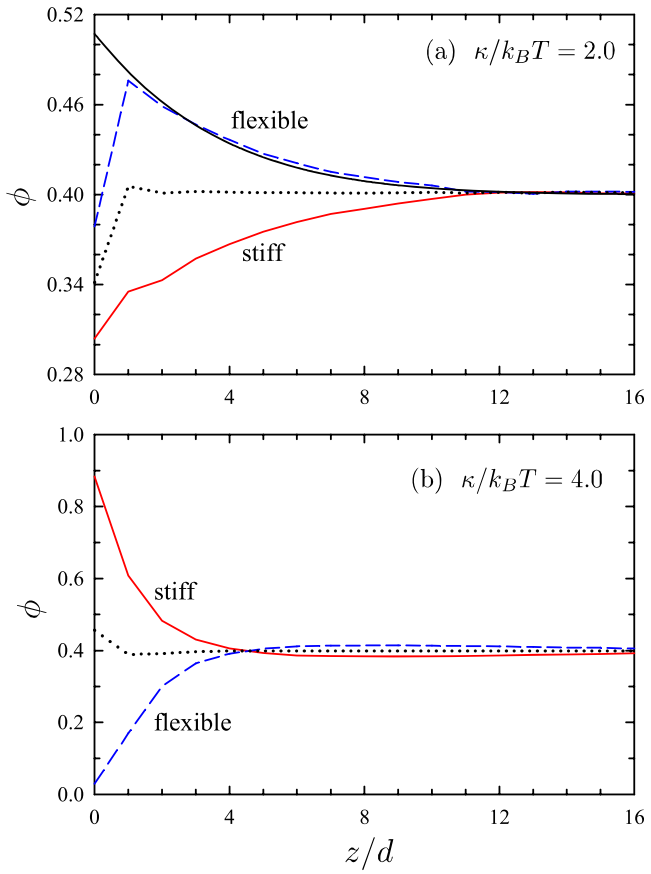

Figure 12. Analogous plots to those of Figure 5 but with the wall potential turned off (i.e., $w(z) = 0$). The black curve in panel (a) denotes the fit $\phi_f(z) = 0.19F_\rho(Z) + 0.4$.

https://doi.org/10.1021/acs.macromol.1c01805
Macromolecules 2021, 54, 10100−10109

orientations. We suspect that these weak packing effects are responsible for the decreasing excess in flexible polymers observed in Figure 7b for $\kappa \gtrsim 3k_BT$. Nevertheless, it is not until after the surface transition, where the bonds next to the wall develop nematic order in the $x-y$ plane (i.e., $S(0) \gg P(0)/3$) that the packing effects are sufficient to induce a surface preference for the stiff polymers.

Immediately following the first surface transition, we do observe concentration profiles in Figure 5b that are qualitatively similar to those of Kumar et al.[22,27] In particular, there is an excess of stiff polymers adjacent to the wall followed by a slight excess of flexible polymers further away. However, the onset of this behavior does not occur until the conformational asymmetry is considerably higher than that considered by Kumar et al., and when it does happen, the degree of order is much stronger. Not only is the amplitude of the segregation larger, the excess of stiff chains also extends further into the melt. Although the orientational order parameter calculated by Kumar et al.[22] cannot detect broken symmetry in the $x-y$ plane, it does show that the tendency for bonds to orient parallel to the wall vanishes within one monomer diameter of the wall, whereas in Figure 6b, it extends to about $z \approx 4d$. These differences become even more pronounced beyond the second surface transition. It is difficult to understand how our results could be so different from theirs, given the similarity of the MC simulations.

Kumar et al.[22,27] modeled the wall as a hard surface and the polymers as tangentially connected hard spheres. As was the case here, their model lacked attractive interactions and included a large amount of free volume, even more than in our model. In real liquids (or melts), attractions combined with limited free volume render them relatively incompressible. As a result, the density of a liquid phase tends to be just slightly less than that of the solid phase. The polymer melts in the simulations, on the other hand, were highly compressible, given that the total concentration near the wall deviated considerably from the bulk density. Note that we are referring to volume density, which would be obtained by a convolution of the distribution of monomer centers in their plots with the concentration profile of an individual monomer. In any case, the resulting compressibility may render their behavior unusually sensitive to model details. Indeed, in similar simulations by Yethiraj,[30] where conformational asymmetry was created by adding short branches to one component rather than changing its bending energy, the surface segregation was reversed by simply adding athermal interactions with the wall or between the monomers. In a relatively incompressible melt, the total energy of these athermal interactions would remain approximately constant and thus should not significantly affect the segregation. It was for this precise reason that we added a field, $w(z)$, to maintain a uniform density across the simulation box.

To assess whether the use of a field accounts for the large differences between our simulations and theirs, we ran several simulations with $w(z) = 0$. Figure 12 shows the resulting concentration profiles, $\phi_s(z)$ and $\phi_f(z)$, which can be compared to those in Figure 5. The tendency to form a nematic layer at the wall is somewhat enhanced because the stiff polymers are able to pack more densely, but we still observed a clear preference for flexible polymers at conformational asymmetries typical of experiment (e.g., $\kappa \lesssim 2k_BT$). The bulk concentration in the simulations of Kumar et al. was typically 40% of the maximum density corresponding to close-packed spheres, which is much lower than the 80% in our simulations. Therefore, we also tried some simulations with $\phi_{bulk} = 0.4$ and $w(z) = 0$, but still the behavior remained vastly different. Our simulations did employ a different bending energy for the stiff polymers, but Kumar et al. already established that their results were not particularly sensitive to the form of the bending energy.[22] The only remaining distinction is that their simulations employed an off-lattice model, but it is doubtful that this can account for the conflicting differences in behavior, especially considering that we used an fcc lattice. If the behavior is, in fact, this sensitive to model details, then one has to be leery of any coarse graining. The implication is that simulations, as well as theoretical calculations, may require realistic atomistic models.

Another more palatable possibility for the differences is nonequilibrium effects. Kumar et al. did report asymmetries in their profiles about the center of their simulation box, which they resolved by including MC swaps between the flexible and stiff chains. Still, there could be other nonequilibrium effects that went undetected. In general, they only equilibrated their simulations until there were no overlaps among monomers,[22] which strikes us as insufficient. Entropic segregation is understood to be a relatively weak effect, and thus good equilibration will be particularly important. This would be especially true for the small degrees of conformational asymmetry studied by Kumar et al. Given the simplification afforded to us by the lattice, as well as 25 years of computer development, we were able to perform orders of magnitude more MC steps during our equilibration. On top of that, we restricted our study to a modest chain length of $N = 40$, long enough to expect polymeric behavior but short enough to allow reasonably fast MC dynamics. Although equilibration was much less of an issue for us, we nevertheless performed numerous tests to confirm that our results were generally free of nonequilibrium effects. We paid particular attention to the average end-to-end vectors and repeated simulations with different initial configurations. The most significant example of metastability was the interval of $4.9 \lesssim \kappa/k_BT \lesssim 6.9$ in Figure 2. However, this is to be expected given that the bulk needs to break isotropic symmetry to nucleate the nematic phase. On the other hand, the symmetry is already broken in the presence of a surface, and so metastability will be less of an issue. Still, to be safe, we ran some of our simulations more than an order of magnitude beyond the point where the profiles appeared to be well equilibrated.

Our simulations are the first to confirm the profile shape in eq 8 predicted by Wu et al.[26] The prediction assumes small conformational asymmetry and large N, but nevertheless, Figures 5a and 12a show it to be reasonably accurate for a large segment length ratio of 1.4 and a relatively small polymerization of $N = 40$. The amplitude of the profile is different depending on whether the simulations were performed with or without a field, but that is to be expected. The field required to maintain uniform polymer density resembles a Dirac delta function at $z = 0$, and the amplitude of the segregation is affected by the local details at the surface. The fact that our results agree with eq 8 is further evidence that our simulations are free of nonequilibrium effects. We also note that the same simulation model with even longer chains reproduced analogous mean-field predictions for entropic segregation in bidisperse melts.[7]

On the other hand, our results do not agree with the fluctuation-corrected calculation of Stepanow and Fedorenko,[29] which predicts a surface preference for the polymers with the larger statistical segment length. Although they claim that their results are qualitatively consistent with the MC simulations

https://doi.org/10.1021/acs.macromol.1c01805
Macromolecules 2021, 54, 10100−10109

of Kumar et al., there is, in fact, one major difference. The calculation predicts the excess, $\phi_{ex}(z)$, to extend into the melt a distance comparable to $\overline{R}_0$, whereas the range in the MC simulations is only on the monomer scale. We note that the calculation by Stepanow and Fedorentko hinges on an assumption regarding the boundary condition used for their effective single-chain Green's function. Motivated, in part, by the Silberberg argument,[16] they used a reflecting boundary. However, the Silberberg argument does not extend to blends with conformational asymmetry, and indeed, Wu et al.[26] showed that the reflecting boundary transforms to a Robin boundary condition.

As expected, packing effects were greatly reduced for the soft surface characteristic of a polymer/air interface. This is evident by the weak orientational order in Figure 10 relative to that of Figure 6b for the hard wall (note the different scales for the vertical axes) and by the fact that the order was insufficient to form a nematic wetting layer. The excess of flexible polymers for $0 \gtrsim z \gtrsim \overline{R}_0$ is still consistent with the profile in eq 8 predicted by Wu et al.,[26] provided that κ is not too large. However, their SCFT calculation would not be able to account for the thin outer layer ($z \lesssim 0$) rich in stiff chains that tend to be parallel to the surface, simply because it is based on Gaussian chains. Nevertheless, this feature could undoubtedly be accounted for by an SCFT calculation based on worm-like chains.[39]

The fact that the width of the surface profile, w_s, has such a significant effect is a warning that entropic segregation could be sensitive to multiple underlying factors. This may explain some of the confusion in the literature. We note, for example, that there are different ways of introducing conformational asymmetry. Although, in the Gaussian chain model, there is nothing beyond the statistical segment length, a, to control conformational asymmetry, in the more realistic worm-like chain model, the statistical segment length, $a = \sqrt{2l_p l_c}$, can be varied by changing the persistence length, l_p, or by changing the contour length of a segment, l_c. In other words, one can vary the bending modulus of the polymer or alternatively the aspect ratio (i.e., length vs cross-sectional diameter) of the segments. As Carignano and Szleifer[28] have demonstrated, these changes will not necessarily result in equivalent behavior. The inclusion of short branches is yet another way of modifying the statistical segment length.[24,30]

It is likely that entropic segregation is more complicated than initially anticipated. We will only find out by carefully comparing the different sources of conformational asymmetry. This will probably best be done with further simulations and theory, where it is possible to ensure that the blends are athermal and completely free of any enthalpic bias between the different polymers.

SUMMARY

Athermal binary blends of linear polymers with equal molecular volume but different stiffness were studied using lattice Monte Carlo simulations. The flexible polymers were modeled as freely jointed chains, while the stiff polymers had an adjustable bending modulus, κ. The effect of κ on the conformational asymmetry between the flexible and stiff polymers is illustrated in Figure 3. At asymmetries typical of experiment ($\kappa \lesssim 2k_BT$), the blends exhibited a single-phase isotropic state, but at sufficiently extreme asymmetries ($\kappa \gtrsim 5k_BT$), the blends macrophase-separated into an isotropic phase rich in flexible polymers and a nematic phase rich in highly extended stiff polymers. Focusing on the isotropic state, we examined entropic surface segregation at neutral surfaces.

We found that it is generally the flexible (i.e., more compact) polymers that segregate to hard walls (i.e., polymer/solid boundaries). Furthermore, their excess was consistent with the concentration profile in eq 8 predicted by Wu et al.[26] However, just prior to the bulk isotropic−nematic transition, a symmetry-breaking surface transition occurred at $\kappa \approx 3.9k_BT$, resulting in the formation of a thin nematic wetting layer rich in stiff polymers. This was then followed by a second surface transition at $\kappa \approx 4.5k_BT$, where the order of the nematic layer suddenly increased and its thickness started to rapidly diverge, nucleating the bulk nematic phase.

Distinctly different behavior was observed for soft surfaces (i.e., polymer/air boundaries). They instead exhibited a thin outer region rich in stiff polymers with a thicker inner region rich in flexible polymers, as depicted in Figure 9. The integrated excess of the flexible polymers generally dominated that of the stiff polymers, as illustrated in Figure 11. Although the stiff polymers in the outer region tended to be parallel to the surface, their concentration was too low to develop nematic order. As a consequence, there were no surface transitions and the surface did not nucleate the bulk nematic phase.

Our lattice MC simulations are consistent with experiments,[17−21] DFT calculations,[23,24] SCFT calculations,[2526] and off-lattice MD simulations,[32] but they are markedly inconsistent with the off-lattice MC simulations by Kumar and coworkers.[22,27] This is highly surprising given that our model is essentially just a lattice version of their model. If the lattice is indeed responsible for such vastly different behavior, then one should be concerned that entropic surface segregation may be hypersensitive to model details, implying the possible need for realistic models that include atomistic details. We believe that this is likely not the case. Instead, we suggest that Kumar et al. may not have equilibrated their system sufficiently to reveal the weak effects of entropic segregation. Concerned with this possibility, we took particular care to do so, which was aided by our use of a lattice, our choice of a modest chain length of N = 40, and the many intervening years of computer development. Nevertheless, further study of their off-lattice model will be necessary to verify if insufficient equilibration is the correct explanation for the differences in behavior.

AUTHOR INFORMATION

Corresponding Authors

Russell K. W. Spencer − *Department of Chemical Engineering, Department of Physics & Astronomy, and Waterloo Institute for Nanotechnology, University of Waterloo, Waterloo, Ontario N2L 3G1, Canada;* orcid.org/0000-0002-4814-9010; Email: r6spence@uwaterloo.ca

Mark W. Matsen − *Department of Chemical Engineering, Department of Physics & Astronomy, and Waterloo Institute for Nanotechnology, University of Waterloo, Waterloo, Ontario N2L 3G1, Canada;* orcid.org/0000-0003-2099-0892; Email: mwmatsen@uwaterloo.ca

Complete contact information is available at: https://pubs.acs.org/10.1021/acs.macromol.1c01805

Notes

The authors declare no competing financial interest.

https://doi.org/10.1021/acs.macromol.1c01805
Macromolecules 2021, 54, 10100−10109

■ ACKNOWLEDGMENTS

The authors thank Sanat Kumar and Marcus Müller for their useful discussions. Computational resources were provided by Compute Canada.

■ REFERENCES

(1) Binder, K. Surface effects on polymer blends and block copolymer melts: Theoretical concepts of surface enrichment, surface induced phase separation and ordering. *Acta Polym.* **1995**, *46*, 204−225.
(2) Kumar, S. K.; Vacatello, M.; Yoon, D. Y. Off-lattice Monte Carlo simulations of polymer melts confined between two plates. *J. Chem. Phys.* **1988**, *89*, 5206−5215.
(3) Yethiraj, A.; Hall, C. K. Monte-Carlo simulation of polymers confined between flat plates. *Macromolecules* **1990**, *23*, 1865−1872.
(4) Kumar, S. K.; Vacatello, M.; Yoon, D. Y. Off-lattice Monte Carlo simulations of polymer melts confined between two plates. 2. Effects of chain length and plate separation. *Macromolecules* **1990**, *23*, 2189−2197.
(5) Bitsanis, I.; Hadziioannou, G. Molecular dynamics simulations of the structure and dynamics of confined polymer melts. *J. Chem. Phys.* **1990**, *92*, 3827−3847.
(6) Pai-Panandiker, R. S.; Dorgan, J. R.; Pakula, T. Static Properties of Homopolymer Melts in Confined Geometries Determined by Monte Carlo Simulation. *Macromolecules* **1997**, *30*, 6348−6352.
(7) Mahmoudi, P.; Forrest, W.; Beardsley, T. M.; Matsen, M. W. Testing the universality of entropic segregation at polymer surfaces. *Macromolecules* **2018**, *51*, 1242−1247.
(8) Wu, D. T.; Fredrickson, G. H.; Carton, J.-P.; Ajdari, A.; Leibler, L. Distribution of chain ends at the surface of a polymer melt: Compensation effects and surface tension. *J. Polym. Sci., Part B: Polym. Phys.* **1995**, *33*, 2373−2389.
(9) Müller, M.; Steinmüller, B.; Daoulas, K. C.; Ramírez-Hernández, A.; de Pablo, J. J. Polymer-solid contacts described by soft, coarse-grained models. *Phys. Chem. Chem. Phys.* **2011**, *13*, 10491−10502.
(10) Matsen, M. W.; Mahmoudi, P. Segregation of chain ends to the surface of a polymer melt. *Eur. Phys. J. E: Soft Matter Biol. Phys.* **2014**, *37*, No. 78.
(11) Mahmoudi, P.; Matsen, M. W. Segregation of chain ends to the surface of a polymer melt: Effect of surface profile versus chain discreteness. *Eur. Phys. J. E: Soft Matter Biol. Phys.* **2016**, *39*, No. 78.
(12) Mahmoudi, P.; Matsen, M. W. Entropic segregation of short polymers to the surface of a polydisperse melt. *Eur. Phys. J. E: Soft Matter Biol. Phys.* **2017**, *40*, 86.
(13) Blaber, S.; Mahmoudi, P.; Spencer, R. K. W.; Matsen, M. W. Effect of chain stiffness on the entropic segregation of chain ends to the surface of a polymer melt. *J. Chem. Phys.* **2019**, *150*, No. 014904.
(14) Zhao, W.; Zhao, X.; Rafailovich, M. H.; Sokolov, J.; Composto, R. J.; Smith, S. D.; Russell, T. P.; Dozier, W. D.; Mansfield, T.; Satkowski, M. Segregation of chain ends to polymer melt surfaces and interfaces. *Macromolecules* **1993**, *26*, 561−562.
(15) Hill, J. A.; Endres, K. J.; Mahmoudi, P.; Matsen, M. W.; Wesdemiotis, C.; Foster, M. D. Detection of Surface Enrichment Driven by Molecular Weight Disparity in Virtually Monodisperse Polymers. *ACS Macro Lett.* **2018**, *7*, 487−492.
(16) Silberberg, A. Distribution of conformations and chain ends near the surface of a melt of linear flexible macromolecules. *J. Colloid Interface Sci.* **1982**, *90*, 86−91.
(17) Sikka, M.; Singh, N.; Karim, A.; Bates, F. S.; Satija, S. K.; Majkrzak, C. F. Entropy-driven surface segregation in block copolymer melts. *Phys. Rev. Lett.* **1993**, *70*, 307−310.
(18) Sikka, M.; Singh, N.; Bates, F. S.; Karim, A.; Satija, S.; Majkrzak, C. F. Surface segregation in model symmetric polyolefin diblock copolymer melts. *J. Phys. II* **1994**, *4*, 2231−2248.
(19) Scheffold, F.; Budkowski, A.; Steiner, U.; Eiser, E.; Klein, J.; Fetters, L. J. Surface Phase Behavior in Binary Polymer Mixtures. II. Surface Enrichment from Polyolefin Blends. *J. Chem. Phys.* **1996**, *104*, 8795−8806.
(20) Tretinnikov, O. N.; Ohta, K. Surface Segregation in Stereochemically Asymmetric Polymer Blends. *Langmuir* **1998**, *14*, 915−920.
(21) Tretinnikov, O. N. Surface Segregation in Polymer Blends of Minimal Difference in the Components Surface Energy. *Macromol. Symp.* **2000**, *149*, 269−275.
(22) Kumar, S. K.; Yethiraj, A.; Schweizer, K. S.; Leermakers, F. A. M. The effects of local stiffness disparity on the surface segregation from binary polymer blends. *J. Chem. Phys.* **1995**, *103*, 10332−10346.
(23) Fredrickson, G. H.; Donley, J. P. Influence of broken conformational symmetry on the surface enrichment of polymer blends. *J. Chem. Phys.* **1992**, *97*, 8941−8946.
(24) Tripathi, S.; Chapman, W. G. Microstructure and Thermodynamics of Inhomogeneous Polymer Blends and Solutions. *Phys. Rev. Lett.* **2005**, *94*, No. 087801.
(25) Donley, J. P.; Fredrickson, G. H. Influence of Conformational Asymmetry on the Surface Enrichment of Polymer Blends II. *J. Polym. Sci., Part B: Polym. Phys.* **1995**, *33*, 1343−1351.
(26) Wu, D. T.; Fredrickson, G. H.; Carton, J.-P. Surface Segregation in Conformationally Asymmetric Polymer Blends: Incompressibility and Boundary Conditions. *J. Chem. Phys.* **1996**, *104*, 6387−6397.
(27) Yethiraj, A.; Kumar, S.; Hariharan, A.; Schweizer, K. S. Surface segregation in polymer blends due to stiffness disparity. *J. Chem. Phys.* **1994**, *100*, 4691−4694.
(28) Carignano, M. A.; Szleifer, I. Surface Segregation in Diblock Copolymers and Polymer Blend Thin Films. *Europhys. Lett.* **1995**, *30*, 525−530.
(29) Stepanow, S.; Fedorentko, A. A. Surface Segregation of Conformationally Asymmetric Polymer Blends. *Phys. Rev. E* **2006**, *73*, No. 031801.
(30) Yethiraj, A. Entropic and Enthalpic Surface Segregation from Blends of Branched and Linear Polymers. *Phys. Rev. Lett.* **1995**, *74*, 2018−2021.
(31) Gramsbergen, E. F.; Longa, L.; de Jeu, W. H. Landau theory of the nematic-isotropic phase transition. *Phys. Rep.* **1986**, *135*, 195−257.
(32) Nikoubashman, A.; Register, R. A.; Panagiotopoulous, A. Z. Sequential Domain Realignment Driven by Conformational Asymmetry in Block Copolymer Thin Films. *Macromolecules* **2014**, *47*, 1193−1198.
(33) Vassiliev, O. N.; Matsen, M. W. Fluctuation effects in block copolymer melts. *J. Chem. Phys.* **2003**, *118*, 7700−7713.
(34) Beardsley, T. M.; Matsen, M. W. Universality between Experiment and Simulation of a Diblock Copolymer Melt. *Phys. Rev. Lett.* **2016**, *117*, No. 217801.
(35) Ivanov, V. A.; Rodionova, A. S.; Martemyanova, J. A.; Stukan, M. R.; Müller, M.; Paul, W.; Binder, K. Wall-induced orientational order in athermal semidilute solutions of semiflexible polymers: Monte Carlo simulations of a lattice model. *J. Chem. Phys.* **2013**, *138*, No. 234903.
(36) Nicolaides, D.; Evans, R. Nature of the Prewetting Critical Point. *Phys. Rev. Lett.* **1989**, *63*, 778−781.
(37) Daoulas, K. C.; Harmandaris, V. A.; Mavrantzas, V. G. Detailed Atomistic Simulation of a Polymer Melt/Solid Interface: Structure, Density, and Conformation of a Thin Film of Polyethylene Melt Adsorbed on Graphite. *Macromolecules* **2005**, *38*, 5780−5795.
(38) Lukyanov, A. V.; Likhtman, A. E. Relaxation of surface tension in the free-surface boundary layer of simple Lennard-Jones liquids. *J. Chem. Phys.* **2013**, *138*, No. 034712.
(39) Morse, D. C.; Fredrickson, G. H. Semiflexible Polymers near Interfaces. *Phys. Rev. Lett.* **1994**, *73*, 3235−3238.

https://doi.org/10.1021/acs.macromol.1c01805
Macromolecules 2021, 54, 10100−10109